

**A/C MAGNETIC HYPERTHERMIA OF MELANOMA MEDIATED BY IRON(0)/IRON
OXIDE CORE/SHELL MAGNETIC NANOPARTICLES: A MOUSE STUDY**

by

SIVASAI BALIVADA

B.Sc., Andhra University, India, 2007

A THESIS

submitted in partial fulfillment of the requirements for the degree

MASTER OF SCIENCE

Department of Anatomy & Physiology
College of Veterinary Medicine

KANSAS STATE UNIVERSITY
Manhattan, Kansas

2009

Approved by:
Major Professor
Deryl L Troyer

Copyright

SIVASAI BALIVADA

2009

Abstract

There is renewed interest in magnetic hyperthermia as a treatment modality for cancer, especially when it is combined with other more traditional therapeutic approaches, such as the co-delivery of anticancer drugs or photodynamic therapy. The influence of bimagnetic nanoparticles (MNPs) combined with short external alternating magnetic field (AMF) exposure on the growth of subcutaneous mouse melanomas (B16-F10) was evaluated. Bimagnetic Fe/Fe₃O₄ core/shell nanoparticles were designed for cancer targeting after intratumoral or intravenous administration. Their inorganic center was protected against rapid biocorrosion by organic dopamine-oligoethylene glycol ligands. TCPP (4-tetracarboxyphenyl porphyrin) units were attached to the dopamine-oligoethylene glycol ligands. The magnetic hyperthermia results obtained after intratumoral injection indicated that micromolar concentrations of iron given within the modified core-shell Fe/Fe₃O₄ nanoparticles caused a significant anti-tumor effect on murine B16-F10 melanoma with three short 10-minute AMF exposures. There is a decrease in tumor size after intravenous administration of the MNPs followed by three consecutive days of AMF exposure. These results indicate that intratumoral administration of surface-modified MNPs can attenuate mouse melanoma after AMF exposure. Moreover, intravenous administration of these MNPs followed by AMF exposure attenuates melanomas, indicating that adequate amounts of TCPP-labeled stealth Fe/Fe₃O₄ nanoparticles can accumulate in murine melanoma after systemic delivery to allow effective magnetic hyperthermic therapy in a rodent tumor mode

Table of Contents

List of Figures	vi
Acknowledgements	viii
CHAPTER 1- Background- Melanoma, Magnetic Hyperthermia & Porphyrine tethered stealth coated Iron/Iron oxide core/shell Magnetic Nanoparticles	1
.....	1
Melanoma.....	2
Hyperthermia.....	4
Magnetic Hyperthermia.....	6
Porphyrine tethered stealth coated Iron/Iron oxide core/shell Magnetic Nanoparticles.....	8
CHAPTER 2- Porphyrin tethered stealth coated MNP- in vitro studies on B16-F10 melanoma cells.....	10
Materials & Methods.....	10
Cell lines.....	10
Porphyrin tethered Stealth-Coated (Bi) Magnetic Fe/Fe ₃ O ₄ Nanoparticles.....	10
Determination of iron concentration in MNPs.....	11
Cytotoxicity of Magnetic Nanoparticles on B16-F10 cells.....	11
Prussian blue staining on MNP treated cells.....	12
Statistical analysis.....	12
Results and discussion.....	12
Figures.....	14
CHAPTER-3- Porphyrin tethered stealth coated MNP- in vivo studies on B16-F10 mouse subcutaneous mealnoma model.....	15
Materials & Methods.....	15
Cell lines & Animals.....	15
Porphyrin tethered Stealth-Coated (Bi) Magnetic Fe/Fe ₃ O ₄ Nanoparticles.....	15
Magnetic Heating.....	16
Temperature measurements on mice.....	16
Intratumoral Hyperthermia.....	17
Intravenous administration of MNPs with AMF exposure.....	17

Histological Analysis.....	18
Statistical analysis.....	18
Results	19
Temperature measurements on mice after intramuscular MNP injection.....	19
Intratumoral Magnetic Hyperthermia.....	19
Intravenously administered MNPs and AMF exposure.....	19
Apoptosis assay.....	20
Discussion.....	21
Figures.....	24
References.....	30

List of Figures

Figure 2.1 <i>In vitro</i> cell viability of B16-F10's cultured in medium containing increasing concentrations of MNPs, as measured by iron concentration. *Statistically significant (p-value less than 0.05;two tail ANOVA).....	13
Figure 2.2 B16-F10 cells after overnight incubation with TCPP labeled MNP. A: control B16-F10 cells (without MNP); B: B16-F10 cells incubated with MNP, C:MNP-incubated B16-F10 cells after Prussian blue staining.....	14
Figure 3.1 Graph depicting temperature change at MNP injection site and in body core during AMF exposure, measured with a fiber optic temperature probe.....	24
Figure 3.2 Effect on tumor burden of intratumoral injection of MNPs followed by AMF treatments. Graph depicting average B16-F10 tumor volumes over time in mice which were later injected with either saline or MNPs intratumorally and with or without AMF treatments. *Statistically significant (p-value less than 0.1).....	25
Figure 3.3 Tumor volume comparison of intravenous MNP administration and AMF exposure group with intravenous DMEM (placebo) and intravenous MNP without AMF exposure groups on day 14 and day 18. (not statistically significant).....	26
Figure 3.4 Effect of intravenous injection of MNP and AMF on tumor weight. *Statistically significant (p-value less than 0.1)- between control and IV MNP+AMF groups.....	27
Figure 3.5 Prussian blue staining on tissue sections after the <i>in vivo</i> experiment. A-C: IV MNP + AMF in tumor, lung, and liver, respectively D: IT MNP+AMF tumor (Scale bar =100 μm).....	28

Figure 3.6 Green fluorescence indicates apoptosis positive and blue is DAPI counterstaining. E-G: Apoptosis assay pictures. E: Control tumor section. F: Tumor section with intravenous MNP administration followed by AMF. G: Tumor section with intratumoral MNP administration followed by AMF. (Scale bar =100 μm).....29

Acknowledgements

I would like acknowledge my major professor, Dr. Deryl L.Troyer, for giving me the opportunity to work in his lab for my masters degree. I would like acknowledge my committee members, Dr. Stefan Bossmann and Dr. Viktor Chikan, for their valuable input for my degree program and in my thesis. I would like to thank my lab members, Marla Pyle, Dr.Rajashekar Rachakatla, and Dr. Gwi-Moon Seo, for their help in my project and proofreading of my thesis. I would also like to thank members of Dr. Bossmann's,, Dr.Chikan's and Dr.Tamura's labs, Hongwang, Thilani Samarakoon, Raj Dani, and Dr. Atsushi Kawabata, for their help in my project.

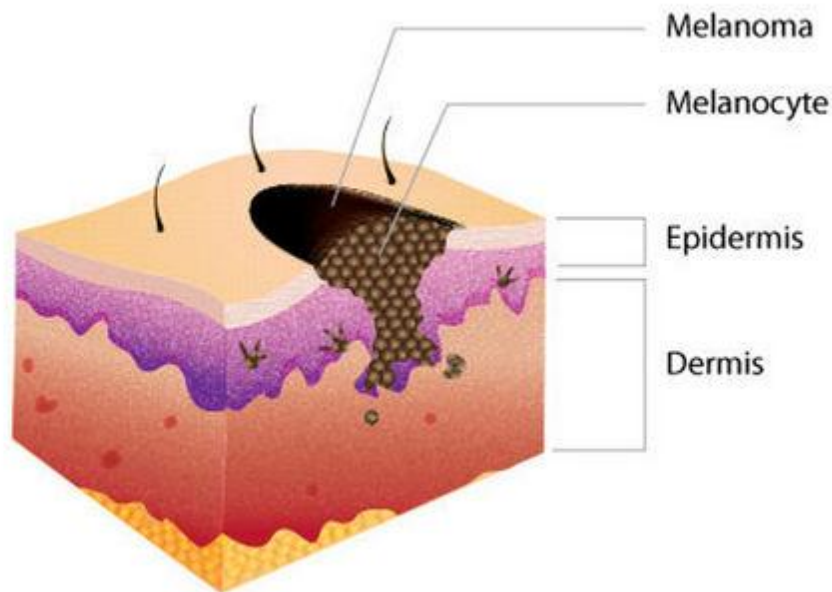
CHAPTER 1 - Melanoma, Magnetic Hyperthermia & Porphyrine tethered stealth coated Iron/Iron oxide core/shell Magnetic Nanoparticles

Recently, questions have surfaced about whether anticancer drug development is headed in the right direction and whether opportunities off the accepted path are being overlooked. [1] Largely due to increasing insight into the series of mutations associated with the development of cancer, drug development has moved into the “molecular target” area. There have been initial successes (e.g. imatinib mesylate for the treatment of chronic myelogenous leukemia and gastrointestinal stromal tumors); however, the genetic complexity and diversity of tumor cells, including the occurrence of cancer stem cells, have prevented molecular targeting from becoming universally successful. Because the progression from normal cell to cancer cell involves numerous genetic mutations, targeting one or even several gene products may be ineffective. Furthermore, many biological processes feature alternate pathways which can be up regulated, if needed, thus thwarting molecularly targeted therapies .[1] To overcome these obstacles, a successful cancer therapy has to combine several approaches. Molecular targeting can be a viable component of this approach. However, other approaches, such as stem cell delivery, hyperthermia, photodynamic therapy, and the design of multifunctional platforms that combine cancer diagnostics and treatment (theranostics) have not received full attention during the last decade.

Melanoma

Melanoma is cancerous disease caused by malignant melanocytes. Melanocytes are mainly present at the junction of epidermis and dermis in skin (Figure 1.1). Melanocytes protect skin by synthesizing melanin pigment, which acts as a photoprotectant by absorbing UV radiation in sunlight. [2] Melanoma most commonly occurs in fair-skinned persons who have substantial sun exposure. [3] Melanoma can occur anywhere on the skin, and regional lymph nodes are the common sites for metastasis. [4] Melanoma can also metastasize to soft tissue, lung, liver, and brain. [3]

Figure 1.1 skin and melanoma



http://www.sciencelearn.org.nz/contexts/you_me_and_uv/sci_media/images/cross_section_of_melanocytes

Superficial spreading melanoma (SSM), nodular melanoma, acral lentiginous melanoma, and lentigo maligna melanoma are the major four types of melanomas. [2, 4] SSM comprises 70% of all melanoma cases; it will be in radial growth phase (growing laterally) for 1-5 years before it starts the invading, vertical growth phase. [2, 4] Nodular melanoma comprises 15% to

30% all melanoma cases. Diagnosis of this melanoma is rather difficult because it lacks a radial growth phase and forms bulge-like tumors. It is usually a dark pigmented melanoma, but around 5% of nodular melanomas lack pigmentation (amelanotic).[4] Acral lentiginous melanoma accounts for 5% of total melanoma cases. It predominantly occurs in dark pigmented persons, where it is found on hands and feet. Prognosis for this disease is worse than for other melanomas.[4] Lentigo maligna melanoma (melanoma *in situ*) represents 5-15% of all melanoma cases and is mostly located on the head and neck.[4] Based on the American cancer staging system(AJCC), primary tumor thickness (Breslow thickness), Clark levels (depths of invasion), mitotic rate, tumor infiltrating lymphocytes, presence of ulceration, blood vessel and lymphatic invasion, and metastasis to lymph nodes are used as prognostic indicators in melanoma.[3] Subcutaneous invasion of melanoma is aggressive in tumor progression. Thus, in the following study, a B16-F10 mouse subcutaneous melanoma model was used.

In its starting stages, melanoma is curable by surgical removal of melanoma tumors, but melanomas in the invasive and metastatic stages are much more difficult to cure.[5] Decarbazine is the most effective drug used for metastatic melanoma therapy; its responsive rate is 10-20%.[5] There are other therapies using IL-2 and Hydroxy urea, but these two are not as effective as decarbazine, and there are several side effects with these therapies.[5] Melanoma is highly radioresistant, so radiotherapy to metastatic melanomas is a poor option.[4, 5] Therefore, novel therapies, which have the capacity to target melanoma with fewer side effects are necessary for metastatic melanoma therapy.

Hyperthermia

Temperature is one of the essential factors controlling cell survival. Changes in temperature can cause structural modifications; sometimes temperature itself is lethal to cells. Hyperthermia is a therapeutic approach to treat cancer treatment which uses higher temperatures which are lethal to cells .[6] Side effects caused by hyperthermia are significantly less than with other cancer treatments, because cancer cells are more sensitive to heat than healthy cells .[7] Hyperthermia is used in combination with other therapies that will improve the prognosis of cancer .[8] There are various types of hyperthermia based on the type of heat administration, such as hot water treatment, microwave, radiofrequency, ultra sound, and alternating magnetic field(AMF). In addition, the type of heat administration may vary: it will be either local, regional (at a specific place), or whole body hyperthermia.[6, 9, 10]

Heat-induced changes in cells finally leads to either apoptosis or necrosis. [11] If cells are exposed to 40-43°C, apoptosis results, while temperatures greater than 45°C cause necrosis. [6] Lipid bilayer and membrane bound ATPases are the least thermally stable components and are most responsible for heat induced tissue necrosis. [11] Increases in temperature will also cause effects such as organelle changes, changes in protein conformation, heat shock protein (HSP) synthesis, and DNA and RNA degradation. [11] Cell death pathways involved in hyperthermia include mitochondria-mediated apoptosis, ER-mediated apoptotic pathways, and necrosis. [6, 11]

Hyperthermia has an additive effect in combination therapies like chemotherapy and radiation therapy.[8] Exposure to heat increases blood flow to the tumors, which improves tissue oxygenation and increases radiosensitivity. [12] In the same way, drug concentration will be less in insufficiently perfused tumors; by increasing the blood flow, hyperthermia increases the drug concentration in tumors. [6] Chemotherapy combined with hyperthermia has showed improved results in tumor models by potentiating the drug effect. [6] To a certain point,hyperthermia

causes cells to overexpress HSPs, thus helping cells to recover from the temperature-induced damage by repairing proteins, synthesizing enzymes that prevent protein aggregation, and degrading severely damaged proteins. [13] But above a threshold temperature increase, inhibition of HSP synthesis occurs. [14] HSPs released from necrotic cancer cells will have attached tumor specific antigens, which aids the innate and adaptive immune response against tumors. [15, 16] Antigen presenting cells (APCs) engulf HSP-protein complexes and subject them to antigen presentation (Srivastava 2002). In this way, hyperthermia causes specific immunity to tumors (immunotherapy combination with hyperthermia. [17-19]

Magnetic Hyperthermia (MHT)

Magnetic hyperthermia (MHT) became a major temperature-based treatment modality by using the magnetic properties of different compounds. The working principle behind MHT is that of exposing MNP to AMF. [20, 21] Two main things involved in MHT are the induction coil, which generates the AMF, and the MNPs, which generate heat when exposed to an AMF. The heat generation depends on the frequency, amplitude, and time exposed to AMF and on Curie temperature, Specific Absorption Rates (SAR), shape, size, dispersity (mono or poly), and type of MNPs. [22]

MNPs create heat either by hysteresis loss or Neel-Brownian relaxation when they are exposed to AMF. [23] Which of these two processes happens depends on MNP size: if the particles are large (multi-domain particles), they will generate heat by hysteresis loss, while small size particles (single domain particles) generate heat by Neel –Brownian relaxations. [23] In multidomain particles hysteresis loss (due to the movement of domain walls) contributes to heating, in single domain particles Neel relaxation(random flipping of spin) and Brownian motion (rotation of entire particles) generates heat. [23, 24] The transition between the two mechanisms occurs between 5-12 nm for various materials, but it also varies with frequency [25].

MNPs vary with the magnetic component in the nanoparticles. Among magnetic nanoparticles, superparamagnetic nanoparticles have more heat generating capacity (more SARs). [22, 26] Iron oxide MNPs are commonly used for MHT in animals because of their biodegradability, low toxicity, and higher SAR values.[27] Apart from MHT, MNPs have different uses in biomedicine like drug delivery, gene delivery, stem cell tracking, MRI, biosensing, cell isolation, cellular proteomics.[28]

For MHT there are some factors of MNPs which must be considered before use in animals: solubility in an aqueous solvent, toxicity, heat distribution to surrounding healthy tissues, blood retention time, and targeting efficiency.[29] Less soluble particles (nanoparticle aggregates) will be easily engulfed by primary immune defensive cells in the vascular system.[29] To reduce aggregation and to increase solubility, MNPs can be coated by different coatings. These coatings will have some negative effect on the MNPs heat generating capacity. If the particles are themselves toxic to healthy cells, there will be more side effects. Several research groups have conducted preclinical studies in animal tumor models by directly injecting MNPs into tumors and observed tumor attenuation [30-33] Tumor specific targeting will be either passive or active. Passive targeting is achieved by the smaller MNPs via enhanced permeability and retention.[22, 34] Tumor vasculature is hyperpermeable compared to healthy tissue vasculatures, which helps the smaller MNPs accumulate in tumor interstitial spaces. [34] The hydrophilic surfactant nature of MNPs also helps in passive targeting by allowing MNPs to avoid plasma protein absorption. [29] Active targeting is achieved by attaching tumor vasculature-specific and tumor cell-specific molecules onto the MNPs. [35] In this way MNPs will be taken up by tumors in higher numbers, thus limiting side effects to healthy tissue. [35] Some researchers have tried to target MNPs to tumors by attaching tumor-specific antibodies.[36] By using cancer targeting MNPs we can image the metastatic sites and we can treat them by using whole body MHT.

Porphyrin tethered stealth coated MNPs Iron(0)/Iron Oxide Core/Shell Magnetic Nanoparticles

Localized hyperthermia is a powerful therapeutic modality. When administered selectively, hyperthermia treatment can be very potent against many types of cancer because it is not based on the intake of drugs by cancer cells, but on the application of heat. A multitude of heat-induced deviations from the “normal” metabolism of a cancer cell can eventually lead to apoptosis (programmed cell death). Although many cancer types are slightly more susceptible to hyperthermia than healthy cells, the latter essentially share the same fate when heated. [29] Therefore, the development of methods to localize hyperthermia to cancer cells remains one of the challenges in this field. This is important when attempting to treat solid tumors within the human body as well as for treatment of metastasizing cancers.

(Bi)magnetic iron/iron oxide core/shell nanoparticles, synthesized by NanoScale Corporation for A/C (alternating current)-magnetic cancer therapy, exhibit superior properties in several areas: The small size ($d < 15$ nm) of these stealth-protected Fe/Fe₃O₄ core/shell nanoparticles will permit passive tumor targeting from the bloodstream by using the EPR (enhanced permeation and retention) effect. [22] The strong paramagnetic iron core has higher magnetization moment and higher saturation magnetization permits MHT with lower concentrations and shorter AMF exposures. The Iron oxide shell surrounding it helps in imaging it through Magnetic Resonance Imaging (MRI). Dopamine on this shell acts as a good anchor for different ligands and increase the stability of MNPs against oxidation. Polyethylene glycol(PEG) ligands attached to this dopamine gives “stealth effect” to MNPs. Tumor cells selectively uptake porphyrins, which they need as prosthetic groups in their elevated sugar metabolism, via over-expression of porphyrin receptors in their cell membranes. [37] There is a strong positive correlation between the cell uptake of a variety of chemically defined, synthetic and natural

porphyrins and their octanol/water distribution coefficients. [38, 39] These findings support the paradigm that there indeed exists a porphyrin uptake mechanism other than endocytosis in cancer cells. The LDL (low-density lipoprotein) receptor, which is over-expressed in cancer cells, has the ability to take up porphyrins as well, either alone or simultaneously with other porphyrin receptors. 4-tetracarboxyphenyl porphyrin (TCPP) molecules are attached to the MNPs to increase the selective accumulation in tumor tissue and to increase the uptake of MNP by cancer cells. In this study detailed below, the intratumoral (IT) and intravenous (IV) core/shell porphyrin-tethered nanoparticle treatment followed by A/C exposure on melanoma growth in a mouse model are examined.

CHAPTER 2 - Porphyrin tethered stealth coated MNPs- in vitro studies on B16-F10 melanoma cells

Materials & Methods

Cell lines

B16-F10 melanoma cells were purchased from ATCC (Manassas, VA) and maintained in DMEM (Dulbecco's Modified Eagle Medium) supplemented with 10% fetal bovine serum (FBS) and 1% penicillin-streptomycin in a humidified 37 °C incubator at 5% CO₂.

Porphyryin tethered Stealth-Coated (Bi) Magnetic Fe/Fe₃O₄ Nanoparticles:

Fe/Fe₃O₄-core/shell nanoparticles were synthesized by NanoScale Corporation and then coated with dopamine-anchored ligands. The diameter of the inorganic cores was 5.4 ± 1.1 nm. Note that the dopamine-anchored tetraethylene glycol ligand (I) and the TCPP-linked dopamine-anchored tetraethylene glycol ligand (II) have been synthesized separately. The binding of the ligands to the Fe₃O₄ layer was achieved in anhydrous tetrahydrofuran (THF) under argon; the molar ratio of ligands I/II was 100/4. We assume a statistical distribution of the ligands at the Fe₃O₄ surface. Assuming a Poisson distribution, 96.4 percent of the Fe/Fe₃O₄ NPs at the chosen ratio feature at least one chemically linked TCPP unit, which will act as "bait" for the B16-F10 cancer cells. The solubility of the organically coated Fe/Fe₃O₄ NPs was determined to be 0.35 mg ml⁻¹ in water and the Specific Adsorption Rate (SAR) at the field conditions described here was 64 ± 2 Wg⁻¹ (Fe).

Determination of iron concentration in MNPs

Iron concentration in MNPs was measured using the Ferrozine-based spectrophotometric iron estimation method. [40] For this method, 50µl of MNPs were diluted to 1 ml with distilled water. MNPs were then lysed by incubating for 2 hours at 65-70 °C after the addition of 0.5 ml of 1.2M HCl and 0.2 ml of 2M ascorbic acid. After incubation, 0.2 ml of reagent containing 6.5mM Ferrozine, 13.1mM neocuproine, 2M ascorbic acid, and 5M ammonium acetate was added and incubated for 30 minutes at room temperature. After 30 minutes, the optical density of the samples was measured using a UV-VIS spectrophotometer at 562 nm. A standard curve was prepared using 0, 0.1, 0.2, 0.5, 1, 2, 5 µg/ml ferrous ammonium sulfate samples. Water with all other reagents is used as blank.

Cytotoxicity of Magnetic Nanoparticles on B16-F10 cells

Potential cytotoxic effects of MNPs were studied by incubating cells in differing concentrations of MNPs. B16-F10 cells were incubated overnight with MNP amounts corresponding to 5, 10, 15, 20, and 25 µg/mL iron. After incubation, the medium was removed, and the cells were washed twice with DMEM. After collection by trypsinization, cells were counted via hemocytometer with Trypan blue staining. This method also allows counting of non-viable cells, since only they allow the blue stain into the cell. All experiments were run in triplicate.

Prussian blue staining on MNP treated cells

B16-F10 cells were incubated overnight with MNP-containing medium. After incubation cells were washed with DMEM two times, harvested with 0.1% trypsin-EDTA, and washed with PBS, followed by centrifugation to remove extra MNPs. These washed cells were replated; after

6 hours cells were fixed with 4% glutaraldehyde. Staining for iron content on these fixed cells was carried out using Perl's Prussian blue staining kit (Polysciences, Inc., Warrington, PA).

Statistical analysis

Statistical analyses were performed by Macanova 4.12 (School of Statistics, University of Minnesota, Minneapolis, MN). The means of the experimental groups were evaluated to confirm that they met the normality assumption. To evaluate the significance of overall differences in live cell numbers between all MNP treated B16-F10 cells, statistical analysis was performed by analysis of variance (ANOVA). A p-value less than 0.05 was considered as significant. Following significant ANOVA, post hoc analysis using least significance difference (LSD) was used for multiple comparisons. Significance for post hoc testing was set at $p < 0.05$.

Results and discussion

MNP toxicity was tested after overnight incubation of B16-F10 cell cultures in 24-well plates with various MNP concentrations, as measured by iron concentration. There was a dose-dependent cytotoxicity of the MNPs. B16-F10 cancer cell viability in the presence of varying concentrations of MNPs is shown in Figure 2.1. The MNPs showed a pronounced cytotoxic effect on B16-F10 cells at $>10 \mu\text{g}$ iron levels ($p\text{-value} < 0.05$). Fixed, MNP-loaded cells are stained with Prussian blue staining (Figure 2.2 A: control B16-F10 cells (without MNP); B: B16-F10 cells incubated with MNP; C: MNP-incubated B16-F10 cells after Prussian blue staining (MNP are blue in color)).

Biocorrosion of these MNPs within the cancer cells (e.g. during endocytosis, within the cytoplasm, or in the cell organelles) causes the formation of free radicals by manifold Fenton-type reactions.[41] Cationic iron (Fe^{+2} , Fe^{+3}) is essential for the cell cycle and for growth, but chelated and unbound iron can induce apoptosis by forming reactive oxygen species (ROS) .[41]

Figures and Tables

Figure 2.1

In vitro cell viability of B16-F10's cultured in medium containing increasing concentrations of MNPs, as measured by iron concentration. *Statistically significant (p-value less than 0.05;two tail ANOVA)

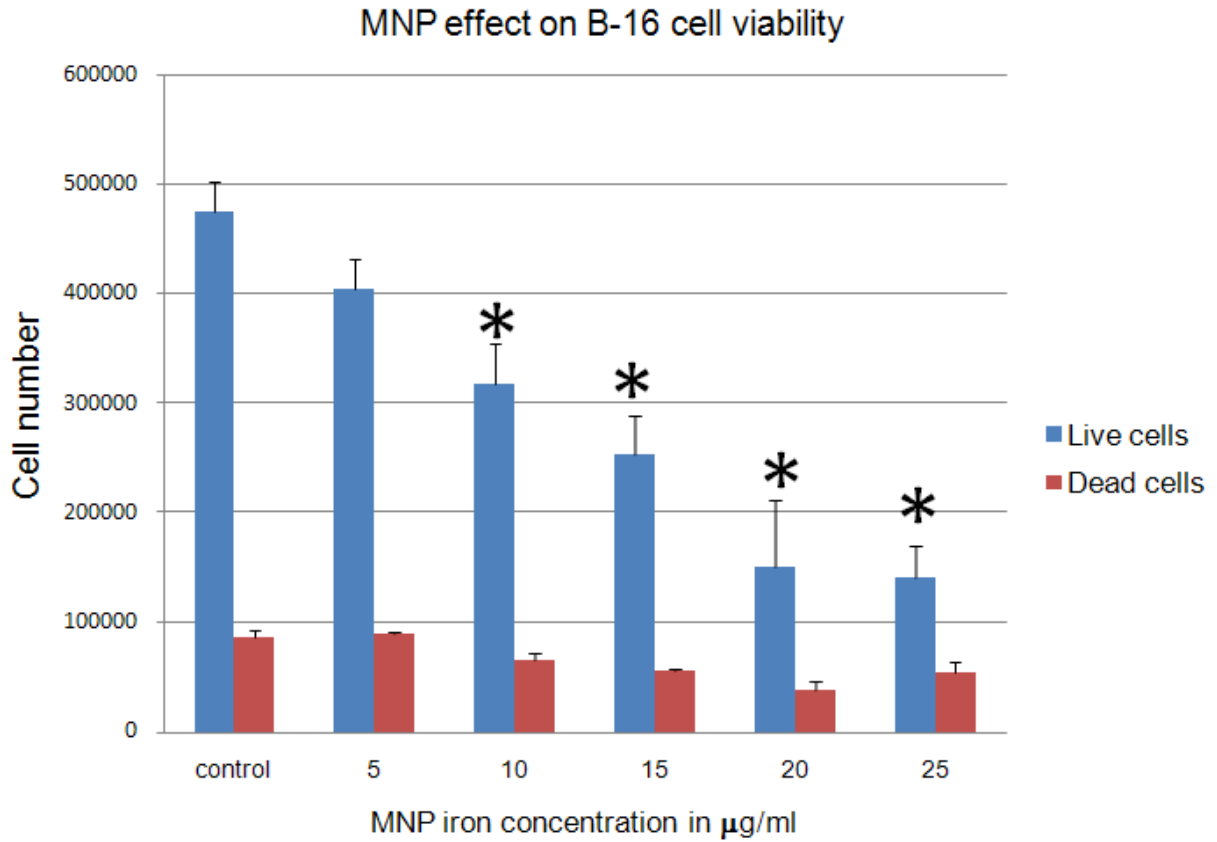
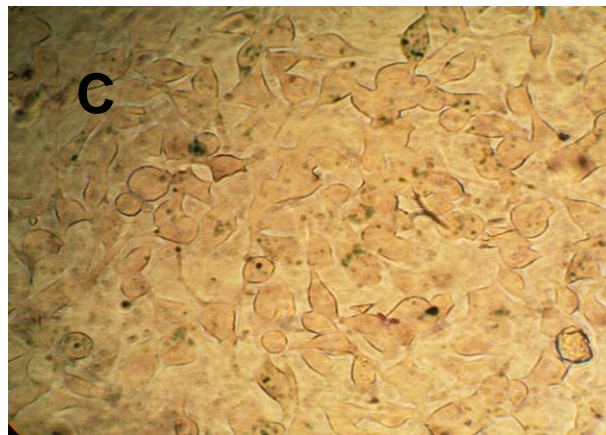
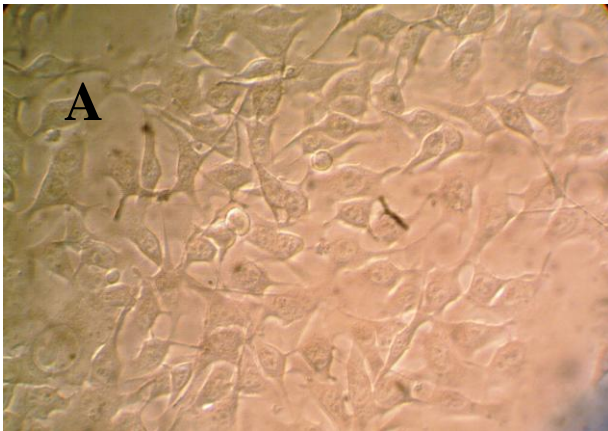


Figure 2.2

B16-F10 cells after overnight incubation with TCPP labeled MNP; A: control B16-F10 cells(without MNP); B: B16-F10 cells incubated with MNP; C:MNP-incubated B16-F10 cells after Prussian blue staining (MNP are blue in color)



CHAPTER 3 - Porphyrine tethered stealth coated MNPs-*In vivo* studies in a B16-F10 subcutaneous melanoma model

Materials & Methods

Cell lines and animals:

B16-F10 melanoma cells were purchased from ATCC (Manassas, VA) and maintained in DMEM (Dulbecco's Modified Eagle Medium) supplemented with 10% fetal bovine serum (FBS) and 1% penicillin-streptomycin in a humidified 37 °C incubator at 5% CO₂.

Six-eight week old female C57/BL6 mice were purchased from Charles River Laboratories (Wilmington, MA). Mice were maintained according to approved institutional IACUC guidelines in the Comparative Medicine Group Facility of Kansas State University. All animal experiments were conducted according to these IACUC guidelines.

Porphyrin-tethered Stealth-Coated (Bi) Magnetic Fe/Fe₃O₄ Nanoparticles

Fe/Fe₃O₄-core/shell nanoparticles were synthesized by NanoScale Corporation and then coated with dopamine-anchored ligands. The diameter of the inorganic cores was 5.4 ± 1.1 nm. Note that the dopamine-anchored tetraethylene glycol ligand (I) and the TCPP-linked dopamine-anchored tetraethylene glycol ligand (II) have been synthesized separately. The binding of the ligands to the Fe₃O₄ layer was achieved in anhydrous tetrahydrofuran (THF) under argon; the molar ratio of ligands I/II was 100/4. We assume a statistical distribution of the ligands at the Fe₃O₄ surface. Assuming a Poisson distribution, 96.4 percent of the Fe/Fe₃O₄ NPs at the chosen ratio feature at least one chemically linked TCPP unit, which will act as "bait" for the B16-F10 cancer cells. The solubility of the organically coated Fe/Fe₃O₄ NPs was determined to 0.35 mg ml⁻¹ in water and the SAR at the field conditions described here was 64 ± 2 Wg⁻¹ (Fe).

Magnetic Heating

The nanoparticles used in these experiments are dominated by Néel relaxation due to the super paramagnetic nature of the iron(0) cores. The hyperthermia apparatus used here has a “heavy duty” induction heater converted to allow measurement of the temperature change of a sample. In the setup, a remote fiber optic probe (Neoptix) is used to monitor the temperature change. The frequency is fixed (366 kHz, sine wave pattern); field amplitude is 5 kA/m. The coil diameter is 1 inch, 4 turns continuously water-cooled. For all *in vivo* experiments, the mice were placed into the induction coil using a specially designed Teflon supporter so that tumors were located exactly in the region of the AMF possessing the highest field density.

Temperature measurements on mice

MNPs containing 100 µg of iron in 100 µl of distilled water were injected into the rear limb muscle of one mouse and the leg was then exposed to AMF for 10 min. A fiber optic temperature probe was inserted intramuscularly at the injection site, and the temperature increase was measured during AMF exposure. At the same time, the body temperature was monitored with a separate temperature probe.

Intratumoral Hyperthermia

Ten mice were transplanted subcutaneously into each rear limb above the stifle with 1×10^6 B16-F10 melanoma cells suspended in 50 μ L PBS. 120 μ L of saline were injected into melanomas on the left leg of all mice and 120 μ L MNPs containing 1 mg Fe/mL were injected into right leg tumors of all mice in three injections on days 4, 5, 6 (total of 360 μ g iron). Both left (saline) and right (MNPs) leg tumors of five of the mice were exposed to AMF for 10 minutes soon after the MNP injections. Tumors on the remaining five mice were not exposed to AMF. Based on this, there were 4 groups which tested the effects of MNPs with and without AMF and of AMF alone: Group 1, Intratumoral saline injection, not exposed to AMF (left legs of first five mice); Group 2, Intratumoral injection of saline, exposed to AMF (left legs of remaining five mice); Group 3, Intratumoral injection of MNPs, not exposed to AMF (right legs of first five mice); Group 4, Intratumoral injection of MNP, exposed to AMF (right legs of remaining five mice). After three AMF exposures, tumor sizes were measured every day with a caliper on days 8 to 14, and tumor volume was calculated using the formula $0.5aXb^2$ (a=longest diameter; b=smaller diameter). After 14 days mice were euthanized, tumors were excised, and tumor weights were measured.

Intravenous administration of MNPs with AMF exposure

On day 0, 3.5×10^5 B16-F10 melanoma cells were injected subcutaneously into the right legs of 27 mice. Mice were randomly divided into three groups: Group I, IV MNPs, no AMF; Group II, IV MNPs, AMF; Group III, DMEM control, no AMF. On days 6, 9, and 11 after tumor cell transplant, MNPs corresponding to 226 μ g of iron were injected intravenously into each mouse in groups I and II. On the same day, DMEM was injected intravenously into group III. For group II, tumors were exposed to AMF for 10 minutes one day after each I.V. MNP

injection (total of three AMF treatments). Tumor sizes were measured using a caliper on days 14 and 18, and tumor volume was calculated as described above. On day 18 all mice were euthanized, tumors were excised, and tumor weights were measured.

Histological Analysis

After euthanizing mice, lung, liver, and tumors were collected and snap frozen. 8-10 μm sections were made in a cryostat (Leitz Kryostat 1720). Staining for iron content on these sections was carried out using Perl's Prussian blue staining kit (Polysciences, Inc., Warrington, PA). Apoptosis was evaluated using a DeadEnd Fluorometric TUNEL kit. (Promega Corp., Madison, WI) following the manufacturer's instructions.

Statistical analysis

Statistical analyses were performed by Macanova 4.12 (School of Statistics, University of Minnesota, Minneapolis, MN). The means of the experimental groups were evaluated to confirm that they met the normality assumption. To evaluate the significance of overall differences in tumor volumes and tumor weights between all *in vivo* groups, statistical analysis was performed by analysis of variance (ANOVA). A p-value less than 0.1 was considered as significant. Following significant ANOVA, post hoc analysis using least significance difference (LSD) was used for multiple comparisons. Significance for post hoc testing was set at $p < 0.1$. All the tumor volumes and weight data were represented as mean +/- standard error (SE) on graphs.

Results

Temperature measurements on mice after intramuscular MNPs injection

We observed 11 °C temperature increase subcutaneously at the MNP injection site within 10 minutes of AMF exposure. There was no increase in core body temperature (Figure. 3.1). These data demonstrate specific magnetic hyperthermia. However, we did not directly measure temperature change in tumors during experiments because the necessary skin opening for the probe caused leakage of the gelatinous melanoma tumor parenchyma, introducing increased potential variability in tumor volumes.

Intratumoral Magnetic Hyperthermia

After three AMF exposures, tumor sizes were measured from days 8 to 14; the comparison is shown in Figure. 3.2. We identified decreased tumor size in tumor-bearing mice treated with MNPs+AMF. The tumors with MNPs+AMF showed a significant reduction in tumor volume at 8, 9, 11, & 14 days ($p < 0.1$) compared to the saline treated group. A decrease in size with only MNP treatment (no AMF) relative to the saline controls was also noted; however, this decrease was not significant. Since earlier intramuscular injections and optical probe measurements revealed hyperthermia after AMF, the probable cause for the tumor attenuation shown here is local hyperthermia.

Intravenously administered MNPs and AMF exposure

Tumor-bearing mice with intravenously injected MNPs were exposed to AMF treatments three times and after 18 days were euthanized. Tumor weights were obtained and compared to controls (Figure 3.4). A significant decrease in tumor weight ($p < 0.1$) was observed in the intravenous MNPs+AMF group and was most likely due to heat generated from MNPs in

tumors, based on earlier optical probe experiments in anesthetized mice. Some tumor weight decrease was also observed in intravenous MNPs without AMF treatment. On days 14 and 18, tumor volumes were recorded and were attenuated in the mice with MNPs with AMF; however this was not significant (Figure 3.3). After tumors were harvested and sectioned, MNPs in tumor sections and other tissues were identified as Prussian blue positive cells in tumor bearing mice intravenously injected with MNPs (Figure 3.5 A-D).

Apoptosis assay

Histological analysis after apoptosis assay with the modified TUNEL assay showed the most apoptotic positive cells in the intratumoral MNP +AMF treatments (Figure 3.6C), intermediate apoptosis levels in mice that received intravenous MNPs+AMF (Figure 3.6B), and the fewest apoptotic cells in the saline+AMF group (Figure 3.6A).

Discussion

The major finding of this study was that there is a significant decrease in tumor size after systemic (intravenous) administration of low (microgram iron content) amounts of the porphyrin-tethered MNPs and AMF exposure compared to tumors in animals given intravenous DMEM. There are very few reports of tumor reduction after superparamagnetic nanoparticles are given this way, so the attainment of tumor attenuation here is a significant finding. We have found the MNPs in the melanomas, indicating that the porphyrins attached to them facilitate MNP uptake. As already discussed, cancer cells over-express porphyrin receptors, because they require more porphyrins as prosthetic groups in their elevated sugar metabolism than normal cells. [37] Tumor localization of MNPs by urokinase plasminogen activator receptor (uPAR) is reported by Yang, Mao *et al.*[42]

Intratumoral magnetic hyperthermia results showed that microgram amounts of iron delivered by the core-shell Fe/Fe₃O₄ nanoparticles caused an antitumor effect on melanoma with short-time AMF exposures (10 min.). This is a clear improvement with respect to current protocols, which are defined by milligram amounts of MNPs and much longer exposure times, usually 30 minutes. [30] We have also observed a trend toward decreased tumor size after MNP administration without AMF exposure. This is not surprising, since our *in vitro* work indicated that the MNPs have a pronounced cytotoxic effect on B16-F10 cells. Minamimura *et al.* gave intratumoral iron oxide MNP injections and noted that their MNPs alone exerted a noticeable anti-melanoma effect. [43] In the study reported here, the effect of MNPs alone is most probably due to the biocorrosion of the MNPs and the subsequent release of iron(II) and iron(III) cations, which is known to cause cell damage via iron(II/III)-enhanced chemistry of reactive oxygen species (ROS). [44] Since the MNPs remain active *in vivo* for 2-3 days, biocorrosion will most likely occur within the cancer cells (e.g. during endocytosis, within the cytoplasm, or in the cell

organelles). Thus, we propose a two-pronged effect: magnetic hyperthermia and the additional generation of free radicals by manifold Fenton-type reactions.[44]

It must be noted that there are significant amounts of iron in lungs and liver, as indicated by Prussian blue staining (Figure. 3.5). Despite this widespread distribution of MNPs *in vivo*, we emphasize that we did not have any fatalities due to the blocking of arteries or exposure to AMF. This may be due to the fact that the AMF was only applied to the melanoma region, preventing unwanted hyperthermia in other tissues. Minimal side effects after systemic administration of MNPs are corroborated by other work testing superparamagnetic NP for MRI capability and possible toxic effects. Wiegand *et al.* showed that 250 or 500 nm ferrofluid given intravenously to normal rabbits resulted in normal serum iron and enzymes for liver and kidney function at 1-72 hours after administration [45]. Kim *et al.* showed that silica over-coated magnetic nanoparticles of 50 nm size did not cause apparent toxicity or alter the blood-brain barrier in mice after four weeks [46].

The findings reported here indicate that ligand-modified MNPs given systemically or intratumorally at low concentrations can significantly attenuate subcutaneous B16-F10 tumors in mice after repetitive short AMF exposure. Hence, it is possible to exploit upregulated porphyrin uptake by cancer cells to facilitate targeted delivery of core/shell bimagnetic nanoparticles. After exposure to an AMF, which itself causes no harm, localized hyperthermia of cancer tissue results in attenuation of the tumor without the undesirable side effects associated with traditional chemotherapy. This approach also circumvents failure of molecularly-targeted approaches due to redundant systems and failure of chemotherapeutic approaches due to cancer cell multidrug resistance. Furthermore, AMF treatment is augmented by the release of iron within the tumor regions due to biocorrosion, increasing the intratumoral concentration of cytotoxic reactive

oxygen species. Thus, localized hyperthermia after systemic administration of porphyrin labeled stealth MNPs may hold promise for future clinical therapy of melanomas.

Figures and Tables

Figure 3.1

Graph depicting temperature change at MNP injection site and in body core during AMF exposure, measured with a fiber optic temperature probe.

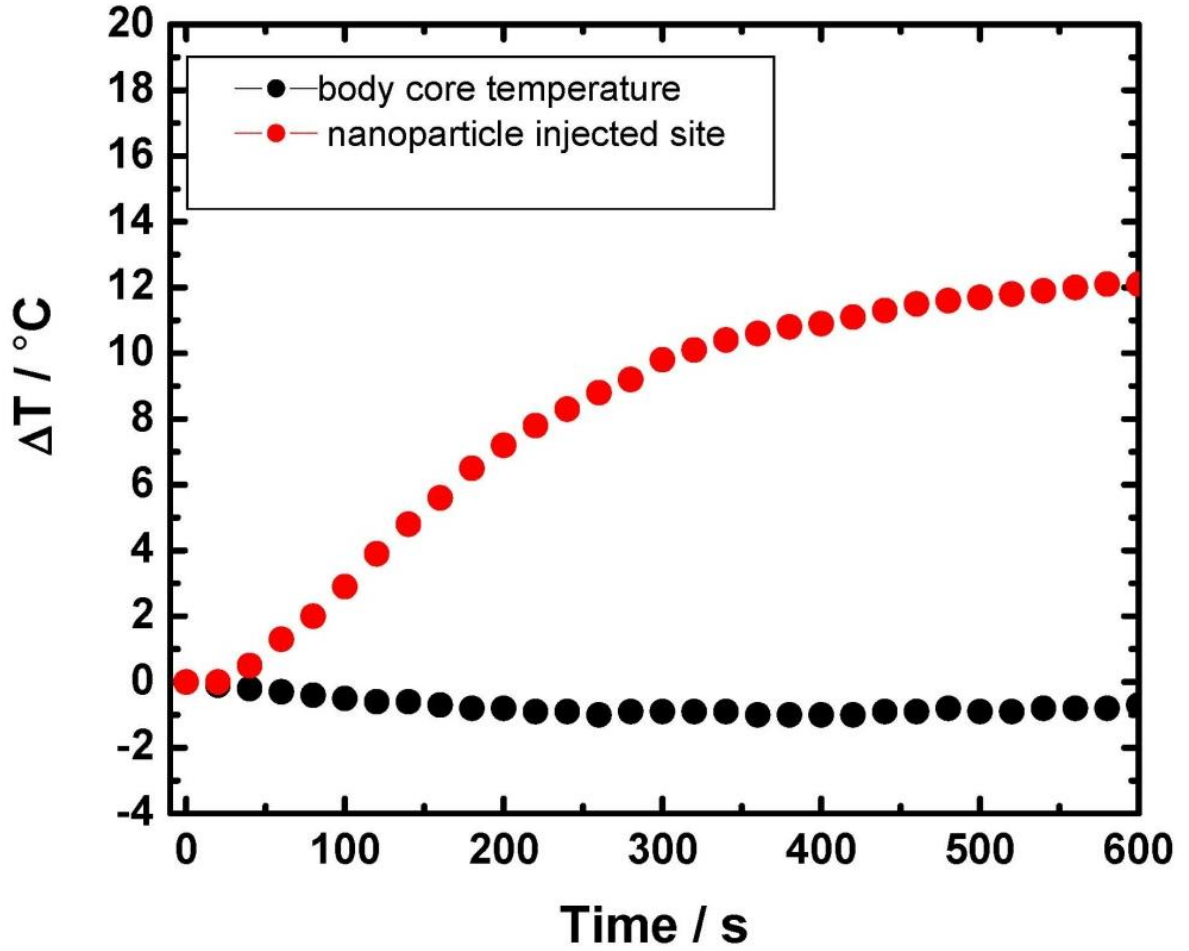


Figure 3.2

Effect on tumor burden of intratumoral injection of MNPs followed by alternating magnetic field (AMF) treatments. Graph depicting average tumor volumes over time of B16-F10 tumor bearing mice which were later injected with either saline or MNP intratumorally and with or without AMF treatments. *Statistically significant (p-value less than 0.1).

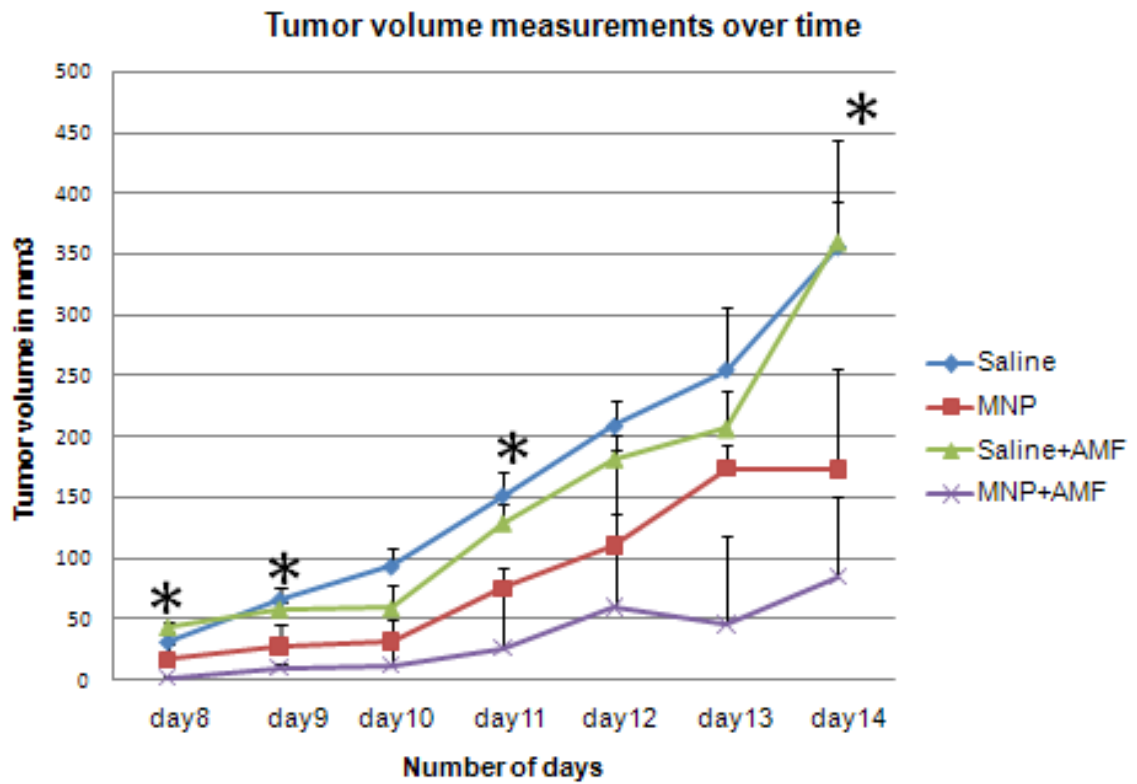


Figure 3.3

Tumor volume comparison of intravenous MNP administration and AMF exposure group with intravenous DMEM (placebo) and intravenous MNP without AMF exposure groups on day 14 and day 18. (Not statistically significant)

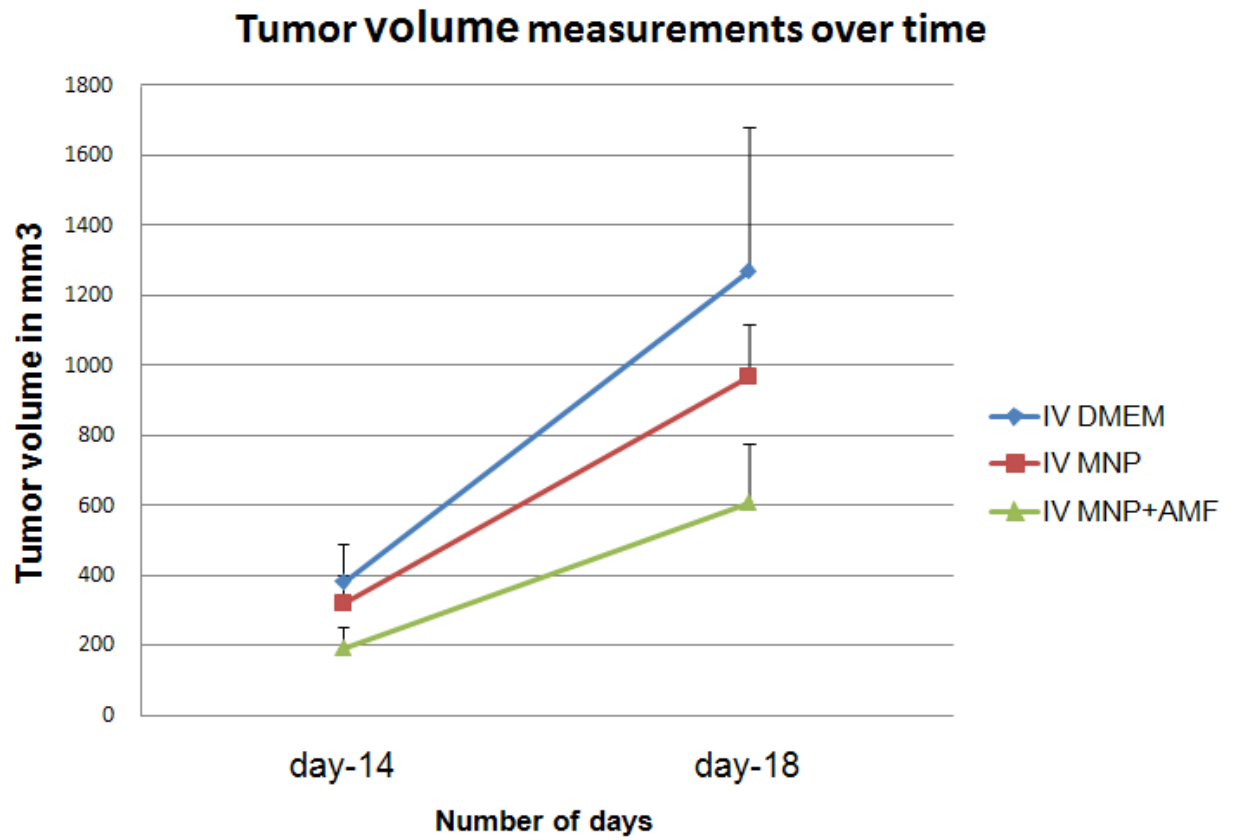


Figure 3.4

Effect of intravenous injection of MNP and AMF on tumor weight. *Statistically significant (p-value less than 0.1) between control and IV MNP+AMF groups.

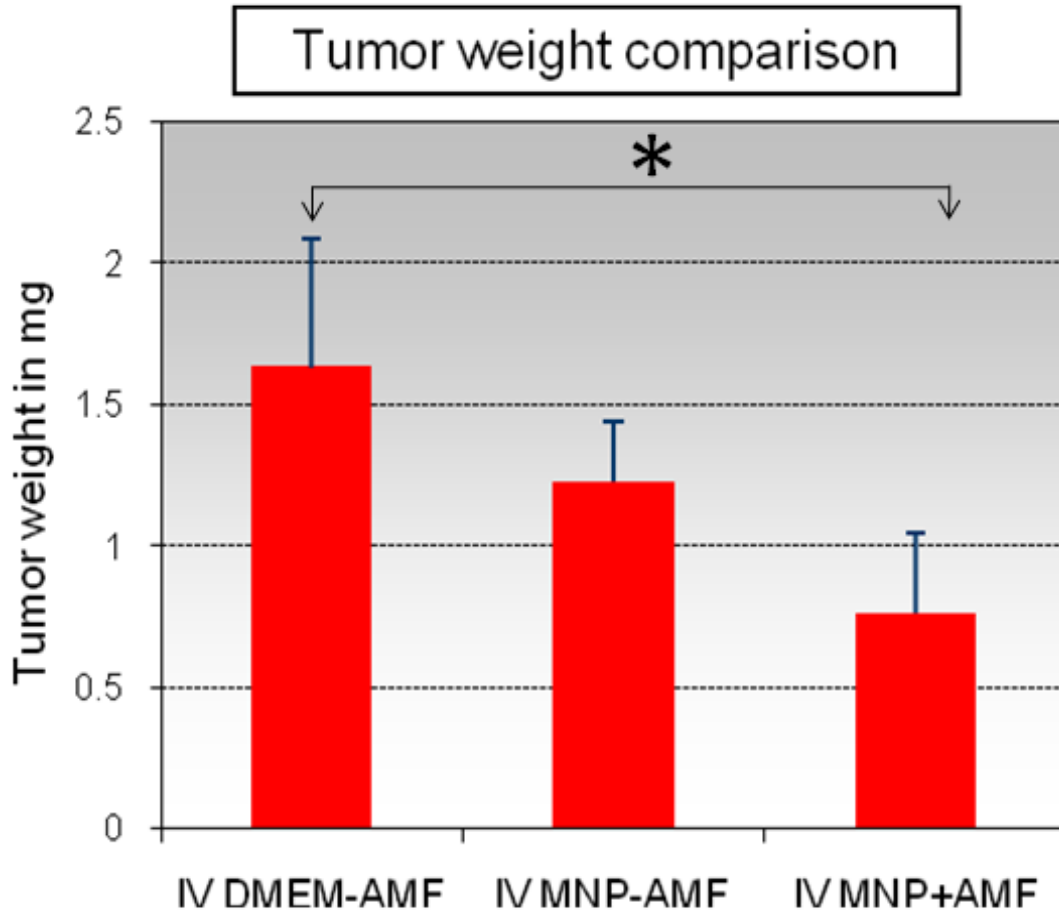


Figure 3.5

Prussian blue staining on tissue sections after the *in vivo* experiment. A-C: IV MNP + AMF in tumor, lung, and liver, respectively D: IT MNP+AMF tumor (Scale bar =100 μm).

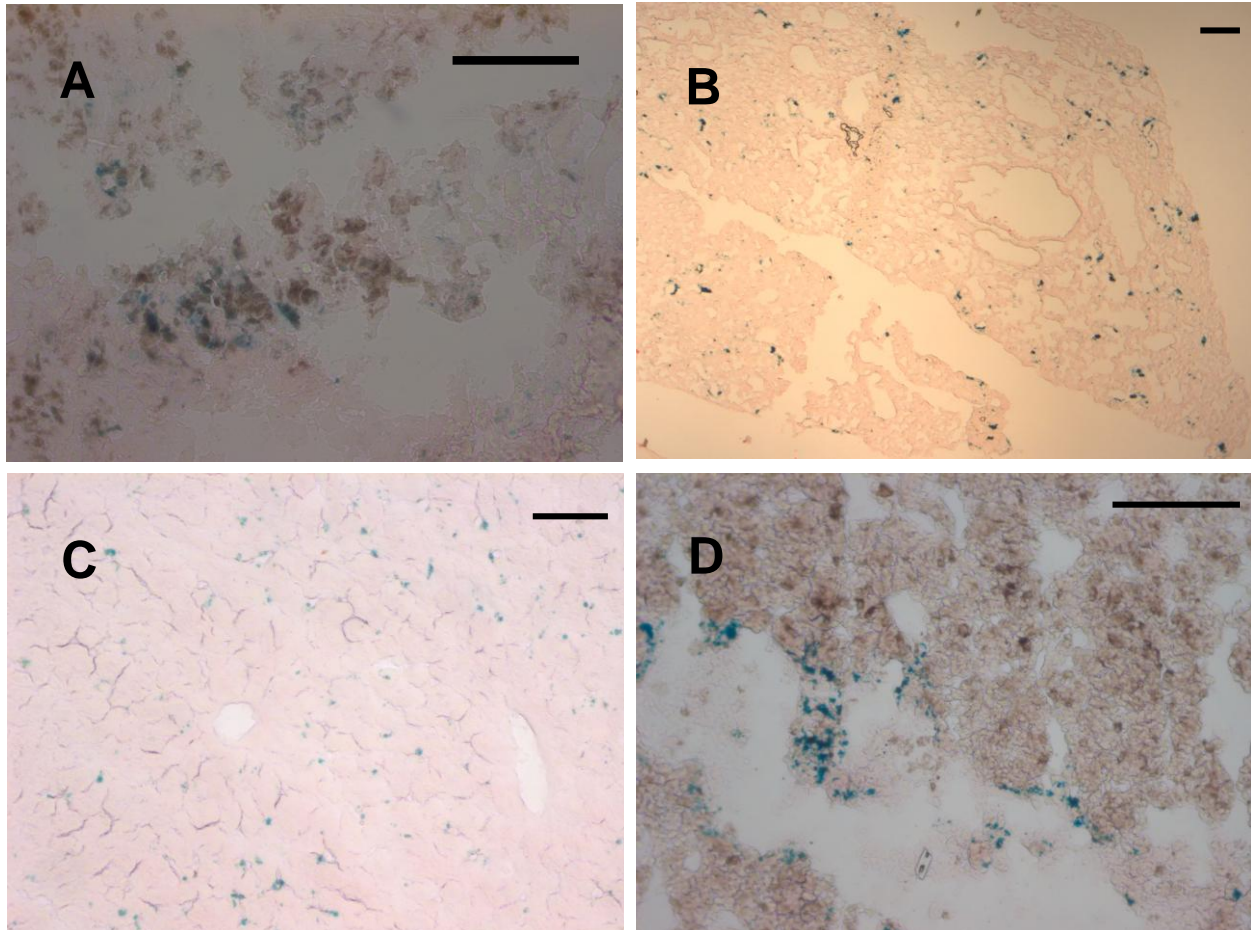
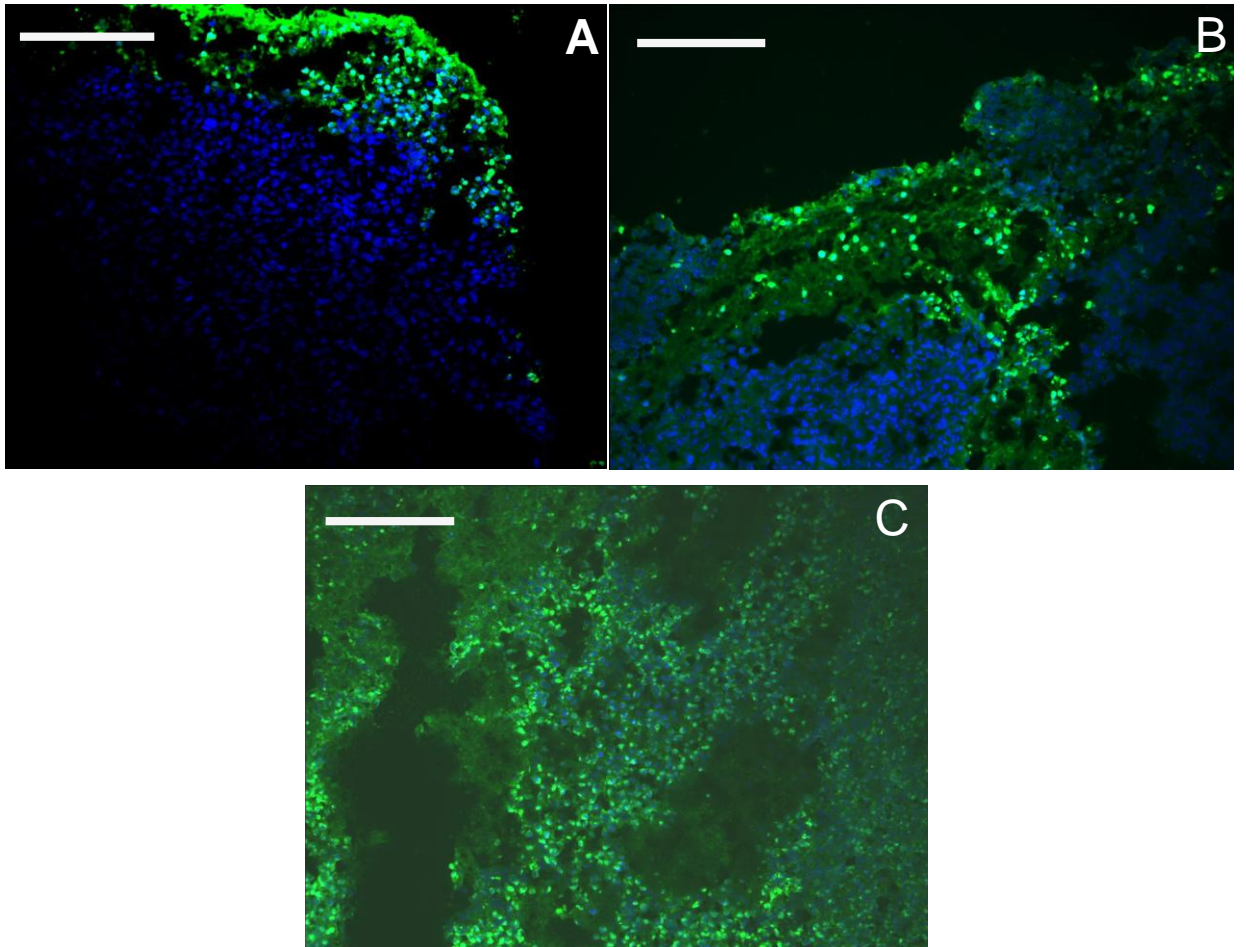


Figure 3.6

Green fluorescence indicates apoptosis positive and blue is DAPI counterstaining. A-C: Apoptosis assay pictures. A: Control tumor section. B: Tumor section with intravenous MNP administration followed by AMF. C: Tumor section with intratumoral MNP administration followed by AMF. (Scale bar =100 μm)



References

1. Hambley, T.W. and W.N. Hait, *Is anticancer drug development heading in the right direction?* Cancer Res, 2009. **69**(4): p. 1259-62.
2. John F. Thompson, D.L.M., Bin B.R. Kroon *Textbook of Melanoma: Pathology, Diagnosis and Management* 2004.
3. AJCC, *AJCC Cancer Staging Manual*. 2004.
4. Ibrahim N, H.F., *Molecular pathogenesis of cutaneous melanocytic neoplasms*. Annual Review of Pathology: Mechanisms of Disease, 2009. **4**: p. 551-579.
5. Gogas, H.J., J.M. Kirkwood, and V.K. Sondak, *Chemotherapy for metastatic melanoma: time for a change?* Cancer, 2007. **109**(3): p. 455-64.
6. van der Zee, J., *Heating the patient: a promising approach?* Ann Oncol, 2002. **13**(8): p. 1173-84.
7. Cavaliere, R., et al., *Selective heat sensitivity of cancer cells. Biochemical and clinical studies*. Cancer, 1967. **20**(9): p. 1351-81.
8. Dewey, W.C., *Interaction of heat with radiation and chemotherapy*. Cancer Res, 1984. **44**(10 Suppl): p. 4714s-4720s.
9. Wust, P., et al., *Hyperthermia in combined treatment of cancer*. Lancet Oncol, 2002. **3**(8): p. 487-97.
10. Falk, M.H. and R.D. Issels, *Hyperthermia in oncology*. Int J Hyperthermia, 2001. **17**(1): p. 1-18.
11. Orgill, D.P., S.A. Porter, and H.O. Taylor, *Heat injury to cells in perfused systems*. Ann N Y Acad Sci, 2005. **1066**: p. 106-18.
12. Song, C.W., et al., *Improvement of tumor oxygenation status by mild temperature hyperthermia alone or in combination with carbogen*. Semin Oncol, 1997. **24**(6): p. 626-32.
13. Subjeck, J.R., et al., *Heat shock proteins and biological response to hyperthermia*. Br J Cancer Suppl, 1982. **5**: p. 127-31.
14. Ito, A., et al., *Antitumor effects of combined therapy of recombinant heat shock protein 70 and hyperthermia using magnetic nanoparticles in an experimental subcutaneous murine melanoma*. Cancer Immunol Immunother, 2004. **53**(1): p. 26-32.
15. Li, Z., A. Menoret, and P. Srivastava, *Roles of heat-shock proteins in antigen presentation and cross-presentation*. Curr Opin Immunol, 2002. **14**(1): p. 45-51.

16. Srivastava, P., *Roles of heat-shock proteins in innate and adaptive immunity*. Nat Rev Immunol, 2002. **2**(3): p. 185-94.
17. Ito, A., et al., *Tumor regression by combined immunotherapy and hyperthermia using magnetic nanoparticles in an experimental subcutaneous murine melanoma*. Cancer Sci, 2003. **94**(3): p. 308-13.
18. Tanaka, K., et al., *Heat immunotherapy using magnetic nanoparticles and dendritic cells for T-lymphoma*. J Biosci Bioeng, 2005. **100**(1): p. 112-5.
19. Dayanc, B.E., et al., *Dissecting the role of hyperthermia in natural killer cell mediated anti-tumor responses*. Int J Hyperthermia, 2008. **24**(1): p. 41-56.
20. Jordan, A., et al., *Presentation of a new magnetic field therapy system for the treatment of human solid tumors with magnetic fluid hyperthermia*. Journal of Magnetism and Magnetic Materials 2001. **225** p. 118-126.
21. Jordan, A., et al., *Inductive heating of ferrimagnetic particles and magnetic fluids: physical evaluation of their potential for hyperthermia*. Int J Hyperthermia, 1993. **9**(1): p. 51-68.
22. Bossmann, S.H., *Nanoparticles for hyperthermia treatment of cancer*. Fabrication and Bio-Application of Functionalized Nanomaterials(ahead to print), 2009.
23. Kotitz, R., P.C. Fannin, and L. Trahms, *Time-Domain Study of Brownian and Neel Relaxation in Ferrofluids*. Journal of Magnetism and Magnetic Materials 1995. **149**: p. 42-46.
24. Pakhomov, A.B., Y.P. Bao, and K.M. Krishnan, *Effects of surfactant friction on Brownian magnetic relaxation in nanoparticle ferrofluids*. J. Appl. Phys, 2005. **97**: p. 10Q305/1-10Q305/3.
25. Mornet, S., et al., *Magnetic nanoparticle design for medical diagnosis and therapy*. J. Mat. Chem. , 2004. **14**: p. 2161-2175.
26. Huber, D.L., *Synthesis, properties, and applications of iron nanoparticles*. Small, 2005. **1**(5): p. 482-501.
27. Gordon, R.T., J.R. Hines, and D. Gordon, *Intracellular hyperthermia. A biophysical approach to cancer treatment via intracellular temperature and biophysical alterations*. Med Hypotheses, 1979. **5**(1): p. 83-102.
28. Xie, J., et al., *Iron oxide nanoparticle platform for biomedical applications*. Curr Med Chem, 2009. **16**(10): p. 1278-94.

29. Shinkai, M., *Functional magnetic particles for medical application*. J Biosci Bioeng, 2002. **94**(6): p. 606-13.
30. Jordan, A., et al., *Effects of magnetic fluid hyperthermia (MFH) on C3H mammary carcinoma in vivo*. Int J Hyperthermia, 1997. **13**(6): p. 587-605.
31. Sato M, Y.T., Ohkura M, Osai Y, Sato A, Takada T, Matsusaka H, Ono I, Tamura Y, Sato N, Sasaki Y, Ito A, Honda H, Wakamatsu K, Ito S, Jimbow K, *N-Propionyl-Cysteaminyphenol-Magnetite Conjugate (NPrCAP/M) Is a Nanoparticle for the Targeted Growth Suppression of Melanoma Cells*. J Invest Dermatol. , 2009.
32. Jordan, A., et al., *The effect of thermotherapy using magnetic nanoparticles on rat malignant glioma*. J Neurooncol, 2006. **78**(1): p. 7-14.
33. Maier-Hauff, K., et al., *Intracranial thermotherapy using magnetic nanoparticles combined with external beam radiotherapy: results of a feasibility study on patients with glioblastoma multiforme*. J Neurooncol, 2007. **81**(1): p. 53-60.
34. Nie, S., et al., *Nanotechnology applications in cancer*. Annu Rev Biomed Eng, 2007. **9**: p. 257-88.
35. Peng, X.H., et al., *Targeted magnetic iron oxide nanoparticles for tumor imaging and therapy*. Int J Nanomedicine, 2008. **3**(3): p. 311-21.
36. Yang, L., et al., *Single chain epidermal growth factor receptor antibody conjugated nanoparticles for in vivo tumor targeting and imaging*. Small, 2009. **5**(2): p. 235-43.
37. Kannagi, R., *Molecular mechanism for cancer-associated induction of sialyl Lewis X and sialyl Lewis A expression-The Warburg effect revisited*. Glycoconj J, 2004. **20**(5): p. 353-64.
38. Oenbrink, G., P. Jurgenlimke, and D. Gabel, *Accumulation of porphyrins in cells: influence of hydrophobicity aggregation and protein binding*. Photochem Photobiol, 1988. **48**(4): p. 451-6.
39. Ben-Dror, S., Bronshtein, I., Wiehe, A., Röder, B., Senge, M. O. and Ehrenberg, B. , *On the Correlation Between Hydrophobicity, Liposome Binding and Cellular Uptake of Porphyrin Sensitizers*. Photochem. Photobiol, 2006. **82** p. 695-701.
40. Riemer, J., et al., *Colorimetric ferrozine-based assay for the quantitation of iron in cultured cells*. Anal Biochem, 2004. **331**(2): p. 370-5.
41. Papanikolaou, G. and K. Pantopoulos, *Iron metabolism and toxicity*. Toxicol Appl Pharmacol, 2005. **202**(2): p. 199-211.

42. Yang, L., et al., *Molecular imaging of pancreatic cancer in an animal model using targeted multifunctional nanoparticles*. *Gastroenterology*, 2009. **136**(5): p. 1514-25 e2.
43. Minamimura, T., et al., *Tumor regression by inductive hyperthermia combined with hepatic embolization using dextran magnetite-incorporated microspheres in rats*. *Int J Oncol*, 2000. **16**(6): p. 1153-8.
44. Winterbourn, C.C., *Toxicity of iron and hydrogen peroxide: the Fenton reaction*. *Toxicol Lett*, 1995. **82-83**: p. 969-74.
45. Wiegand, S., et al., *Evaluation of the tolerance and distribution of intravenously applied ferrofluid particles of 250 and 500 nm size in an animal model*. *J Drug Target*, 2009. **17**(3): p. 194-9.
46. Kim, J.S., et al., *Toxicity and tissue distribution of magnetic nanoparticles in mice*. *Toxicol Sci*, 2006. **89**(1): p. 338-47.